Engineering Structures 231 (2021) 111735

Contents lists available at ScienceDirect

Engineering Structures

journal homepage: www.elsevier.com/locate/engstruct

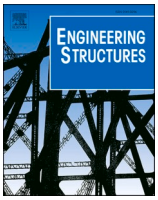

Experimental investigation and analytical modelling of shear strength of thin walled textile-reinforced UHPC beams

Philipp Preinstorfer [a,*], Patrick Huber [b], Tobias Huber [a], Benjamin Kromoser [c], Johann Kollegger [a]

[a] Institute of Structural Engineering, TU Wien, Karlsplatz 13/212-2, 1040 Vienna, Austria
[b] FCP Fritsch, Chiari & Partner ZT GmbH, Marxergasse 1 B, 1030 Vienna, Austria
[c] Institute of Structural Engineering, University of Natural Resources and Life Sciences, Gregor-Mendel-Straße 33, 1180 Vienna, Austria

ARTICLE INFO

Keywords:
UHPC
Carbon textile reinforcement
CFRP rods
T-beam
Shear strength

ABSTRACT

The combination of two high performance materials, ultra-high performance concrete and carbon reinforcement, allows for the construction of efficient, durable thin-walled structural elements. In order to investigate the shear behaviour of such elements a test series on thin-webbed textile reinforced T-beams was planned and carried out at the Institute of Structural Engineering at TU Wien. In the experiments the efficiency of carbon textile reinforcement grids with different impregnation materials used as shear reinforcement was analysed. Furthermore, the shear span to effective depth ratio as well as the effect of prestressing on the shear carrying capacity was investigated. This article describes the experimental programme and shows the test results. The evaluation of the results indicates a higher shear performance of beams with lower-tex sand coated, acrylonitrile-styrene-acrylate copolymers impregnated textile fabrics than with Heavy-Tow grids with an epoxy resin impregnation. For the case of prestressing the carbon fibre reinforced polymer an additional increase of the shear carrying capacity of the thin-walled carbon textile reinforced structures was verified.

1. Introduction

The building construction industry is constantly on the lookout for sustainable, innovative materials and solutions in order to primarily decrease building costs and energy consumption in comparison to classical reinforced concrete. A material that has the potential to meet this requirement in certain areas of applications is textile-reinforced concrete (TRC). TRC is a combination of fine-grained concrete (generally high-performance concrete) and multi-axial textile fabrics (longitudinal and transversal rovings) typically made of aramid, basalt, alkali-resistant glass or carbon fibres. Over the last decade, German research institutes have been the main pioneers in the investigation of this high-performance composite material [1,2]. Recently, the research interest has also sparked in other countries, e.g. [3–5]. In various research projects the material (compression, tension, bond, etc.) as well as structural behaviour (bending, shear, etc.) of TRC using different types of textile fabrics was investigated [6–12] with the results are currently being summarized in a RILEM Technical Committee.

The material is characterized by a high durability, especially for carbon textiles [13], which allows for a reduction of the concrete cover and thus, the construction of slender, lightweight structures with a long estimated service life, particularly suitable for pedestrian bridges [14], shells [15–17] and façade panels [18]. In addition, the resulting weight reduction is of particular interest for the production of precast elements for building constructions [19,20]. Furthermore, it was discovered, that TRC is a suitable material for strengthening of existing structures like shells [21], columns [22], webs of shear critical beams [23,24] and others.

Nowadays, mainly impregnated textiles (preferably carbon and AR-glass) are used as reinforcement. Due to the impregnation, the tensile strength and bond behaviour of the fabrics is essentially enhanced by a better activation of the core filaments [25]. Thus, tensile stresses up to 3500 MPa can be achieved e.g. for carbon textiles. In order to further improve the bond strength of TRC the surface of the rovings can additionally be coated with sand [26]. Beyond that, it is possible to pre-shape the textile elements three-dimensionally preserving the form using an ensuing impregnation. Currently, acrylate and styrene based polymers (easily bent to limited bending radii) and epoxy resins (high stiffness) are the most commonly used impregnation materials [27]. A recent

* Corresponding author.
E-mail address: Philipp.preinstorfer@tuwien.ac.at (P. Preinstorfer).

https://doi.org/10.1016/j.engstruct.2020.111735
Received 13 July 2020; Received in revised form 19 October 2020; Accepted 9 December 2020
Available online 17 January 2021

Nomenclature

a	shear span (distance between the mid-point of the applied load and the mid-point of the support plate)
$a_{tex,w}$	fibre cross-sectional area of shear reinforcement
c	distance from extreme fibre of the cross section to centre of longitudinal reinforcement
b_w	web width
d	effective depth
$f_{c,cube}$	cube compressive strength (b = h = 100 mm)
f_{ct}	tensile strength
$f_{ct,fl}$	flexural tensile strength
$f_{t,tex}$	tensile strength of textile reinforcement
k_b	reduction factor of tensile strength of textile reinforcement due to spalling of the concrete cover
k_T	reduction factor of tensile strength of textile reinforcement due to non-axial loading of textile reinforcement and various other effects
l_b	anchorage length
l_{eff}	span length of the specimen
s	slip
s_r	centre-to-centre distance of fibre strands
w	crack width
z	lever arm
A_c	cross-sectional area of the beam
A_{rov}	cross-sectional area of a fibre strand
A_{tex}	cross-sectional area of textile reinforcement
E_c	young's modulus of concrete
E_{tex}	young's modulus of textile reinforcement
F_{tex}	normal force in textile fabric
F_c	normal force in concrete
$F_{c,spal}$	normal force in concrete at initiation of a spalling
P	prestressing force
T	bond flow
U_{tex}	circumference of fibre strand
V	shear force
V_{Exp}	maximum shear strength in the tests
V_{spal}	shear force at initiation of a spalling
$V_{R,c}$	shear strength contribution of the concrete
$V_{R,tex}$	shear strength contribution of textile fabrics
α_{cr}	inclination of shear crack at location of textile fabric
β_{cr}	angle of the shear crack
β_{cc}	reduction factor to account for a load introduction $a/d < 3$
ρ_w	shear reinforcement ratio
$\varepsilon_{u,tex}$	breaking strain of textile reinforcement
σ_{cp}	concrete stresses due to prestressing
σ_{tex}	textile reinforcement stress
$\sigma_{tex,eff}$	textile stress that can be transmitted via the shear crack
δ	vertical displacement
δ_b	slip at crack opening
τ_b	bond stress
$_m$	mean
$_{max}$	maximum
$_{test}$	time of testing
$_{eff}$	effective strength under consideration of various degradation parameters
$_c$	concrete
$_{spal}$	spalling
ASA	acrylonitrile-styrene-acrylate copolymers
UHPC	ultra-high performance concrete
CFRP	carbon fibre-reinforced polymer
DIC	digital image correlation
SPO	single-sided textile pull-out

study [28] showed, that the possible reduction of concrete in TRC considerably decreases the cumulative energy demand and environmental impact in some rating categories. In certain areas of application, the ecological footprint lies below that of conventional reinforced concrete. However, this can only be ensured if structures are optimized accordingly and the high-performance materials used are fully utilized [10,20].

In this paper, the structural performance of thin-walled T-beams made of carbon textile reinforcement and ultra-high performance concrete (UHPC) is investigated by means of a test series of 18 shear tests on 9 T-beams. The construction elements tested and presented below could be used in practice as precast ribbed slabs for building constructions. While there are already several studies on the bending behaviour of TRC [10,29], the presented research focused on the little investigated shear behaviour of filigree, exclusively carbon reinforced T-beams. First preliminary results of this study are published in [30]. To complement the described test results this manuscript will focus on the detailed evaluation of the shear carrying capacity of the used textile reinforcement.

2. Experimental programme

2.1. Specimens

To gain a better understanding of the shear behaviour of thin-walled T-beams made of carbon reinforcement (rods and textiles) and UHPC a comprehensive experimental programme was performed. The main investigating parameters consisted of the type of the textile reinforcement grid (impregnation: acrylonitrile-styrene-acrylate copolymers (ASA); type 1 vs. epoxy resin; type 2); different shear reinforcement ratios, the shear span to effective depth ratio a/d, and the thickness of the walls (web and flanges). Furthermore, the effect of prestressing of the carbon fibre reinforced polymer (CFRP) rods on the shear strength of carbon reinforced concrete was analysed. The main parameters are summarized in Table 1.

Three different types of test specimens were produced. Fig. 1 shows the dimensions as well as the reinforcement layouts of the different cross sections used in this study. The height and the width of the upper flange was the same for all specimens and was set to 260 mm and 300 mm respectively. To investigate the effect of different wall thicknesses, the web width was 30 mm for cross section type 1 (see Fig. 1a) and increased to 40 mm for cross sections types 2 and 3 (see Fig. 1b and c). Furthermore, the height of the compression flange (20 vs. 30 mm) as well as the width of the tension flange (100 vs. 120 mm) were varied. Another major difference between cross section type 1 and cross sections types 2 and 3 was the diameter of the used CFRP rods, which was changed from a diameter of 8 mm to a diameter of 10 mm. The only difference between specimens type 2 and specimens of type 3 was that a prestressing force was applied on specimens of type 3. In addition to the CFRP bars a flat carbon textile grid of the same type as the respective shear reinforcement was used as longitudinal reinforcement in the compression and tension flanges of each specimen.

The effective depth d of the textile reinforcement acting in tension is listed in Table 2. The effective depth d of the CFRP rods is shown in Fig. 1. The shear reinforcement consisted of two preformed L-shaped carbon textile grids. The L-shape grids were installed in such a manner that resulted in a straight anchorage in the bottom flange and a longer almost horizontal anchorage in the top flange. Two different types of textiles were used in this study (see Table 4) as shear reinforcement with varying cross sections of the rovings A_{rov}, varying distances between the rovings s_{rov} as well as different impregnation materials. Furthermore,

Table 1
Main parameters of the test specimens.

Specimen	Cross section type (Fig. 1)	b_w [mm]	a/d[1]	Longitudinal reinforcement (CFRP rods)	Shear reinforcement		P_{test} [kN]
					$a_{tex,w}$ [mm²/m]	Type (see Table 4)	
T2.5S30	1	30	2.48	2Ø8	90.0	1	
T3.0S30	1	30	2.95	2Ø8	90.0	1	
T3.5S30	1	30	3.46	2Ø8	90.0	1	
T4.0S30	1	30	3.93	2Ø8	90.0	1	
T2.5S40	2	40	2.52	2Ø10	90.0	1	
T3.0S40	2	40	3.00	2Ø10	90.0	1	
T3.5S40	2	40	3.52	2Ø10	90.0	1	
T4.0S40	2	40	4.00	2Ø10	90.0	1	
T2.5E30	1	30	2.48	2Ø8	190.5	2	
T3.0E30	1	30	2.95	2Ø8	190.5	2	
T3.5E30	1	30	3.46	2Ø8	190.5	2	
T4.0E30	1	30	3.93	2Ø8	190.5	2	
T2.5E40	2	40	2.52	2Ø10	190.5	2	
T3.0E40	2	40	3.00	2Ø10	190.5	2	
T3.5E40	2	40	3.52	2Ø10	190.5	2	
T4.0E40	2	40	4.00	2Ø10	190.5	2	
PT3.0S40	3	40	3.00	2Ø10 + 1Ø10[2]	90.0	1	70.7 + 27.0[2]
PT4.0S40	3	40	4.00	2Ø10 + 1Ø10[2]	90.0	1	70.7 + 27.0[2]

[1] Referred to the CFRP rods.
[2] Rod in the compression chord.

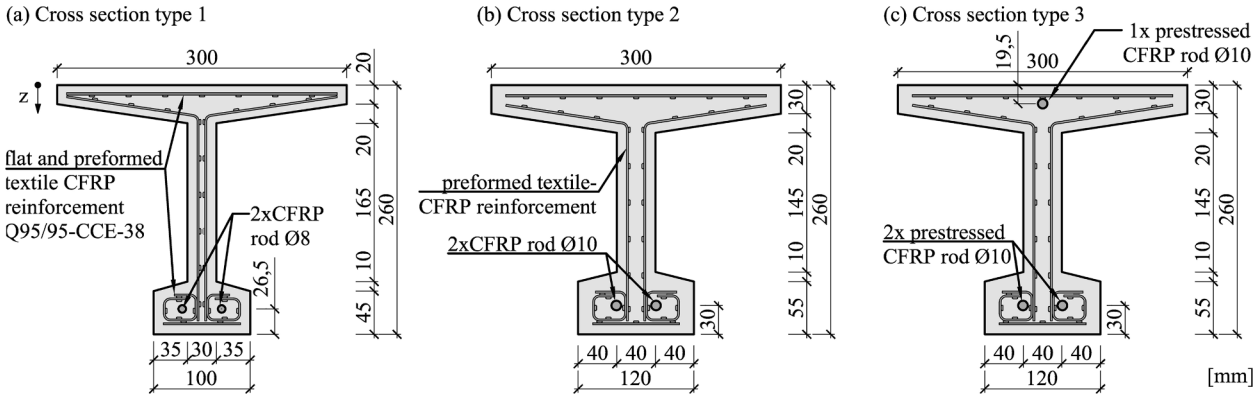

Fig. 1. Dimensions and reinforcement layout of the different types of specimens used in the study.

Table 2
Effective depth d of the rovings of the textile reinforcement in the web and the tension flange.

Shear reinforcement	Q45/45-CCS-20			Q95/95-CCE-38		
Cross section type	n_r	d [mm]	A_{tex} [mm²]	n_r	d [mm]	A_{tex} [mm²]
1	11·2	40/60/80/ 100/120/ 140/ 160/ 180/200/ 220/240	11·1.8	6·2	38/76/ 114/152/ 190/228	6·7.24
	5·2	221/225/ 235/243/ 247	5·7.24	5·2	221/225/ 235/243/ 247	5·7.24
2/3	11·2	43/63/83/ 103/123/ 143/ 163/ 183/203/ 223/243	11·1.8	6·2	47/85/ 123/161/ 199/237	6·7.24
	5·2	221/225/ 235/243/ 247	5·7.24	4·2	218/222/ 233/243	4·7.24
				3	247	10.86

the surface of the textile reinforcement with ASA-impregnation was additionally sand coated. Details of the transverse reinforcement are given in Table 2. The CFRP rods in the type 3 specimens (PTx.xS40) were prestressed in a stressing bed using a conventional prestressing jack by coupling the rod with a steel strand. To improve the bond, the rods in the coupler were notched (for detailed information on the prestressing system see [31]). An additional, prestressed carbon rod was added at the compression flange to avoid cracking due to the arising bending moment caused by the bottom focused pre-tensioning. The prestressing forces measured in the specimens on the day of testing are listed in Table 1. Each test specimen was labelled according to the individual test parameters. The specimen name is composed as follows:

X 0.0 Y 99	
X	reinforcement
	PT:**p**restressed **T**RC
	T: non prestressed **T**RC
0.0	a/d ratio
Y	type of shear textile reinforcement
	S: Q45/45-CCS-20 (A**S**A impregnation)
	E: Q95/95-CCE-38 (**e**poxy impregnation)
99	Web thickness [mm]

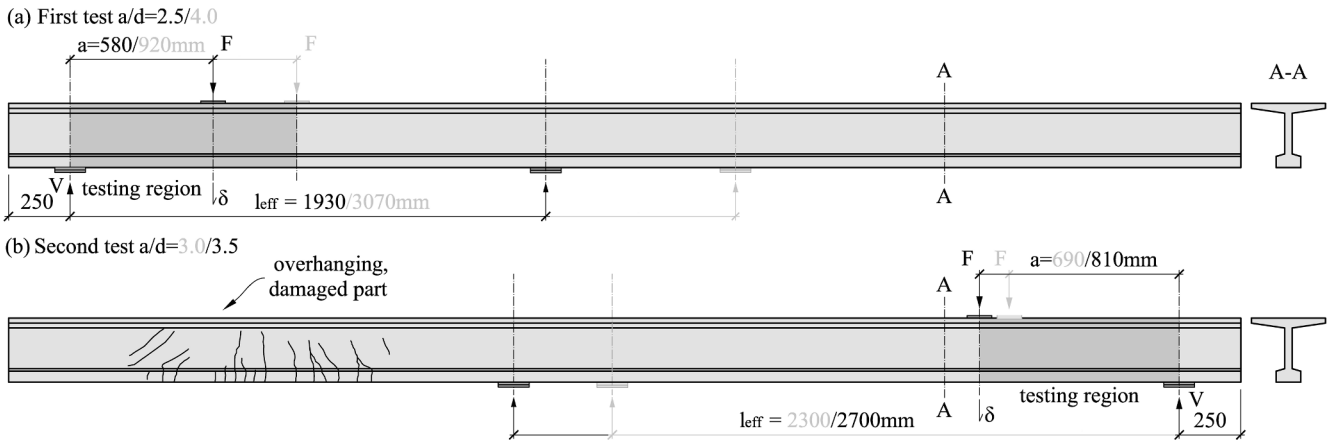

Fig. 2. Test setup of the shear tests: (a) First test (shear span/effective depth ratio a/d = 2.5 or 4.0); (b) Second test (a/d = 3.0 or 3.5) [30]

2.2. Test setup

A simple 3-point bending test setup (see Fig. 2), with an applied single load, was chosen for testing. The load was introduced at specific distances which would ensure clearly defined testing regions, where shear failure could be expected. To investigate the effect of shear slenderness on the shear strength, the position of the load introduction was varied. The tested a/d ratios are listed in Table 1. It was possible to test each specimens twice, since the testing region of the second test was situated in the cantilever section of the first test (see Fig. 2a). For the second test setup, attention was paid to the placement of the entire damaged area from the first test in the cantilever (see Fig. 2b). The ratio between the shear span and the total span was kept constant at 0.3.

2.3. Material properties of used materials

2.3.1. Concrete

All beams were made of UHPC with a maximum aggregate size of 1.6 mm. The material tests were performed immediately after a set of two to four beam loading tests. The mean values of the cube compressive strength (on 100 mm × 100 mm cubes) and the flexural tensile strength varied for all beams between 159.7 and 173.0 MPa and 9.2 and 10.5 MPa, respectively. According to [32] the uniaxial tensile strength was calculated between 4.7 and 5.4 MPa. The material properties of the concrete are summarised in Table 3. One cubic metre of UHPC consisted of approximately 980 kg of quartz sand (one half 0.1–0.5 mm grain size and one half 1.0–1.6 mm grain size), 10 kg of mixing water, 750 kg of cement (CEM I 52.5 N C3A free), 60 kg of superplasticiser, 40 kg of shrinkage compensator and admixture (200 kg stone powder and 310 kg microsilica slurry) and 1 kg of defoamer.

Table 3
Material properties of used UHPC (mean value after 28 days of hardening).

Specimen	$f_{c,cube}$ [1] [MPa]	$f_{c,cube}$ [2] [MPa]	$f_{ct,fl}$ [3] [MPa]	f_{ct} [4] [MPa]	E_c [3] [GPa]
T2.5S30/ T3.5S30 T2.5S40/ T3.5S40	159.7	165.3	10.3	5.3	52.6
T3.0S30/ T4.0S30 T3.0S40/ T4.0S40	162.0	156.8	9.2	4.7	50.0
T2.5E30/ T3.5E30 T3.0E40/ T4.0E40	167.0	159.5	10.5	5.4	53.6
T3.0E30/ T4.0E30 T2.5E40/ T3.5E40	170.0	167.8	10.5	5.4	53.0
PT3.0S40/ PT4.0S40	173.0	158.1	9.8	5.0	49.5

[1] Tested on 100 × 100 mm cubes.
[2] Tested on 40 × 40 mm cubes (fractions from flexural tensile test prism).
[3] Tested on 40 × 40 × 160mm prism
[4] Acc. to [33].

Table 4
Dimensions and material properties of textile reinforcement.

Textile fabric type	Type 1	Type 2
ID	Q45/45-CCS-20	Q95/95-CCE-38
Impregnation material	ASA	epoxy resin
A_{rov} [mm^2 (tex)]	0.90 (1600)	3.62 (6400)
s_{rov} [mm]	20	38
a_{tex} [mm^2/m]	45	95
$f_{t,tex,0}$ [MPa] – warp dir.[1]	1944	3024
$f_{t,tex,90}$ [MPa] – weft dir.[1]	2108	3348
$E_{tex,0}$ [GPa] – warp dir.[1]	212.6	235.1
$E_{tex,90}$ [GPa] – weft dir.[1]	204.9	251.9
$\varepsilon_{u,tex,0}$ [·10^{-3}] – warp dir.[1]	9.2	12.9
$\varepsilon_{u,tex,90}$ [·10^{-3}] – weft dir.[1]	10.3	13.3

[1] Mean value of six tensile tests according to [34].

2.3.2. Textile reinforcement

The material properties and dimensions of the various utilised carbon textile reinforcement are listed in Table 4. The test setup for the determination of the material parameters was chosen according to [34]. The tensile behaviour was linear elastic until reaching the tensile strength [20]. As will be described in detail later, the shape of the textiles plays an important role in the structural behaviour. The cross section of a single fibre strand of the used textiles has an elliptical shape. The connection of the warp and weft strands in the textiles type 2 by warp knitting results in a compression of the fibre strands at the intersection creating a certain regularly repeating asperity on the surface. In the textiles type 1, the connection between the two directions is facilitated by an intersection of the weft roving through the warp roving resulting in no regularly repeating variation in cross-sectional dimensions. Fig. 3 shows a comparison of the two textile fabric types by means of digital 3d-models of the fabrics generated by laser scans.

The bond behaviour of the used textiles was investigated after the shear tests showed pronounced spalling of the concrete cover due to high bond action (see section 3.1ff). A detailed description of the experiments can be found in [35,36]. In contrast to conventional metallic reinforcement bars, carbon textile reinforcement has no standardized test method, as the pull-out test according to RILEM [37], for determining the bond strength. Due to this fact the authors chose the single-sided textile pull-out (SPO)-test based on the work of Lorenz [38], in which a single roving is pulled out of a thin-walled concrete element. Details of the test setup are shown in Fig. 4a.

The thickness of the SPO-test specimens was chosen based on the beam web width of 30 mm. The width of the elements was set to 100 mm and reduced to 20 mm or 38 mm in the anchorage zone, according to

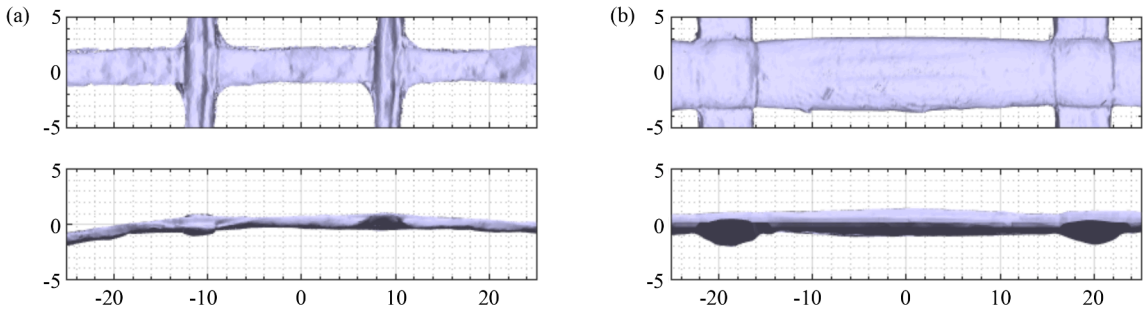

Fig. 3. Geometric properties (3D-model) of the textile fabrics (a) Q45/45-CCS-20, (b) Q95/95-CCE-38 [mm]

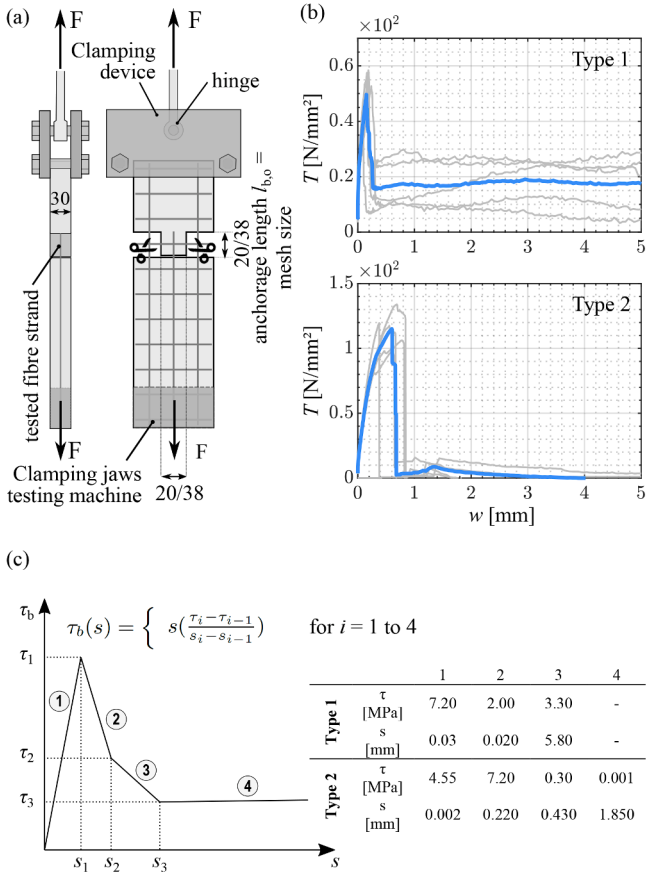

		1	2	3	4
Type 1	τ [MPa]	7.20	2.00	3.30	-
	s [mm]	0.03	0.020	5.80	-
Type 2	τ [MPa]	4.55	7.20	0.30	0.001
	s [mm]	0.002	0.220	0.430	1.850

Fig. 4. Testing of the bond performance of TRC: (a) test setup of a SPO-test; (b) bond flow-crack opening diagram of ASA impregnated textile and epoxy impregnated textile, (c) calculated bond-slip relationship.

adaptions made by Bielak et.al [39], to account for a spalling of the concrete cover due to splitting tensile stresses. The bond length of the roving and the reduced width was chosen to be the mesh size of the grid (20 and 38 mm). In contrast to Lorenz [38], a crack was initiated by placing a PE sheet at the beginning of the bond length in the specimens before casting. This allowed for a more precise testing of the bond length without exceeding the tensile capacity of concrete beforehand. Fig. 4b shows the bond flow T ($=F/l_b$) in relation to the crack opening w for the two tested textile types (5 tests per textile type). The fibre strands with the ASA impregnation and sand-coated surface (textile type 1) reached a maximum mean bond flow of 49.6 N/mm. After reaching the maximum value, the bond flow dropped to 15.7 N/mm remaining at the value while the crack opening increased. The remaining bond strength can be traced back to the friction capacity of the sand-coated surface. The ultimate failure resulted in a total pull-out of the fibre strands in all test specimens without cracking of the concrete matrix. The fibre strands with 6400 tex and an impregnation made of epoxy resin (textile type 2) showed a completely different bond behaviour. The maximal bond flow T of 115.1 N/mm (mean value of 5 tests) surpassed that of the ASA-impregnated textiles. The main bond mechanism acting in this phase can be assigned to a mechanical interlock, which is enabled by the regularly repeating variation in the cross-sectional dimensions [40]. After the maximum bond flow T was reached, a longitudinal crack initiated, leading to a sudden drop to almost zero of the bond flow transmitted in the interface. Minimal slowly decreasing friction remained while the crack opening increased. The cause of the longitudinal cracking can, on the one hand, be traced back to the increased bond flow capacity due to the higher amount of filaments compared to textile type 1, on the other hand to the specific geometric properties of textile type 2, e.g. the elliptical shape of the fibre strand and a wedge effect on account of the regularly repeating variation in cross-sectional dimensions (for further details compare [41]). Furthermore, the epoxy resin impregnation is much stiffer than the ASA impregnation, resulting in a much more pronounced wedge effect. As it will be discussed later, this phenomenon has a significant influence on the shear behaviour of thin-walled beams with textile fabrics as shear reinforcement. In order to describe the bond behaviour, a simple multilinear bond law can be used. Fig. 4c illustrates the details regarding the bond strength and corresponding slip for both textile types. The derivation of the bond-slip relationship from the load-crack opening-diagram can be done either by semi-analytical [42] or numerical methods [43,48].

A difference in the concrete cover of the bond performance test specimens described in this section and the overall shear performance test specimens has to be noted. While the bond stiffness in the uncracked state is not affected significantly by the thickness of the concrete cover, which is supported by the results of the recalculations of the stress state in section 4.1, the bond strength for the epoxy-impregnated textiles may be overestimated due to the bigger concrete cover.

2.3.3. CFRP rods

Sand coated CRFP rods were used as bar reinforcement. The impregnation was made of epoxy resin. The sand coating was achieved by roughing the plain bars, coating them with epoxy resin and subsequently sprinkling them with quartz sand of a grain size between 0.3 and 0.7. This method provides a high bond strength (mean value of approx. 15.0 MPa) and a high bond stiffness (for detailed information on the bond performance see [44]). The material properties for the CFRP rod reinforcement were taken from material tests provided by the producer. The tensile strength of the bars was stated as 2,048 MPa, the modulus of elasticity as 161 GPa and the ultimate strain as 12.72 mm/m.

2.4. Measurements

During testing, continuous measurements of the load, deflections as well as strains on the concrete surface were recorded. In addition, the kinematics (opening and sliding of the crack surfaces) of critical cracks during the experiments could be analysed with the help of digital image

correlation (DIC). The photogrammetric measurement system ARAMIS 4 M from the company GOM with two 4 megapixel cameras (resolution 2,352 × 1,728 pixels) was used. The post-processing of the images was performed with the DIC software GOM Correlate Professional 2016. A random high-contrast speckle pattern was applied to the concrete surface in order for the photogrammetric system to identify an overlapping grid of facets (15 × 15 pixels for the evaluation of crack kinematics). The image acquisition rate of the cameras was changed at specific load steps, and the frequency was increased to 5 Hz just before failure of the specimen occurred.

3. Analysis of shear behaviour

3.1. Description of the failure modes

The shear capacity V_{exp} of all tests is summarized in Table 5. A shear induced failure was observed in all conducted experiments. Fig. 5 shows the crack pattern after failure for the tests with an a/d ratio of 4.0.

Different failure modes were observed throughout the varying series. Thereby, a clear tendency regarding the type of textile reinforcement (used as shear reinforcement) was visible. All tests with an epoxy resin impregnation and a high yarn count (textile type 2; see Table 4) exhibited a distinct spalling of the concrete cover due to longitudinal cracking in the web without a rupture of the textile fabrics (see Fig. 5b). As the bond performance was reduced significantly after initiation of a longitudinal cracking, a sudden loss of stiffness of the system was noticed; see Fig. 6. Subsequent failure occurred due to crushing of the concrete compression strut preceded by a distinct spalling of the concrete cover. The distinct spalling of the concrete cover in the case of epoxy-impregnated textiles is primarily caused by high splitting tensile stresses due to bond action (see section 4.3). A separation of the concrete cover due to the big surface area of textile fabrics is not supported by the data, as the ASA-impregnated textiles exhibited a bigger surface area, while simultaneously no spalling of the concrete was observed in these tests.

The ASA-impregnated TRC-beams (textile type 1) showed a typical flexural-shear crack failure (the critical shear crack formed from a flexural crack) with rupture of the textile fabrics and crushing or splitting of the compression zone near the load introduction. A third failure mode, a shear-tension failure, was observed in the specimen PT3.0S40 (prestressed beam) with an a/d ratio of 3.0. The critical shear crack was formed in the web next to the support leading to a fracture of the textile grid (ASA-impregnation) without spalling of the concrete cover.

3.2. Effect of the influencing parameters

Fig. 7 shows the maximum experimental shear force V_{exp} (values are listed in section 3.1; Table 5) depending on several influencing parameters. In all the tests a clear trend regarding the influence of the shear span to effective depth ratio a/d was visible.

With an increasing a/d ratio, a decreasing shear resistance could be observed. Furthermore, it was noted that a thicker web and flange resulted in an improvement of the shear carrying capacity of around 20% (see Fig. 7a and b). Although the shear performance index $\rho_w \cdot f_{t,tex}$ was more than four times higher for the beams with the textile reinforcement type 2, the difference of the shear carrying capacity only accumulated to 23% (compare Fig. 7a and b). The results showed that the most effective way (especially for the chosen configurations) to improve the shear capacity of carbon reinforced beams is by prestressing the CFRP rods. Although the prestressing force was relatively small (20% of the tensile capacity of the CRFP bars), an improvement of the maximum experimental shear force of 44% was achieved (see Fig. 7c). The various effects and mechanisms leading to the observed shear carrying capacity of the different specimens are discussed in the following sections.

4. Modelling of shear carrying capacity of textile reinforcement

4.1. Measured stress state in textile reinforcement at failure

Specimens reinforced with epoxy impregnated fabrics (type 2) failed at comparably low shear forces in contrast to their high shear performance index $\rho_w \cdot f_{t,tex}$ (more than four times higher than specimens reinforced with ASA-impregnated fabrics; see Table 5). This low efficiency can be traced back to the initiation of a longitudinal cracking in the web at an early stage, causing a spalling of the concrete cover and subsequently leading to a premature failure due to a significant degradation of the bond performance. The initiation of the longitudinal cracking is dependent upon the geometric and mechanic properties of the textile. The stress state in the textile, which allows conclusions on the effectiveness of the reinforcement at initiation of the spalling, can be determined in terms of measured crack-opening at the location of the textile yarns. The development of the crack-opening of the critical shear crack during testing at the place of a representative fibre strand crossing the crack is depicted in Fig. 8 for all tests specimens.

In reference to the bond performance tests described in section 2.3.2, longitudinal cracking is induced at a low crack-opening of the primary

Table 5
Model parameters and results of the testes specimens.

Specimen	$\rho_w \cdot f_{t,tex,90}$ [MPa]	$(d\text{-}c)$ [mm]	$\sigma_{tex,eff}$ [MPa]	β_{cr} [°]	$V_{R,tex}$ (Eq 3) [kN]	V_{exp} [kN]	V_{spal} [kN]	$V_{R,tex}/V_{exp}$ [-]	$V_{R,tex}/V_{spal}$ [-]
T2.5S30	6.32	196.1	1523	40	32.4	49.5	–	0.65	–
T3.0S30	6.32	196.1	1809	51	26.3	37.8	–	0.70	–
T3.5S30	6.32	196.1	1735	46	29.7	35.1	–	0.85	–
T4.0S30	6.32	196.1	1640	40	34.6	35.3	–	0.98	–
T2.5S40	4.74	182.9	1774	44	30.1	55.8	–	0.54	–
T3.0S40	4.74	182.9	1839	40	36.6	46.9	–	0.78	–
T3.5S40	4.74	182.9	1640	38	34.6	44.6	–	0.77	–
T4.0S40	4.74	182.9	1690	42	30.9	40.7	–	0.76	–
T2.5E30	21.26	196.1	1774	57	43.5	55.0	53.7	–	0.81
T3.0E30	21.26	196.1	939	43	37.5	54.4	45.1	–	0.83
T3.5E30	21.26	196.1	1020	47	35.4	41.5	39.5	–	0.90
T4.0E30	21.26	196.1	760	41	32.8	43.2	38.2	–	0.86
T2.5E40	15.95	182.9	1099	46	36.6	70.3	64.2	–	0.57
T3.0E40	15.95	182.9	939	42	36.8	56.4	54.2	–	0.68
T3.5E40	15.95	182.9	939	41	37.4	54.2	43.5	–	0.86
T4.0E40	15.95	182.9	1020	50	30.4	48.3	39.4	–	0.77
PT3.0S40	4.74	182.9	1667	28	52.7	67.3	–	0.78	–
PT4.0S40	4.74	182.9	1761	28	55.0	64.0	–	0.86	–

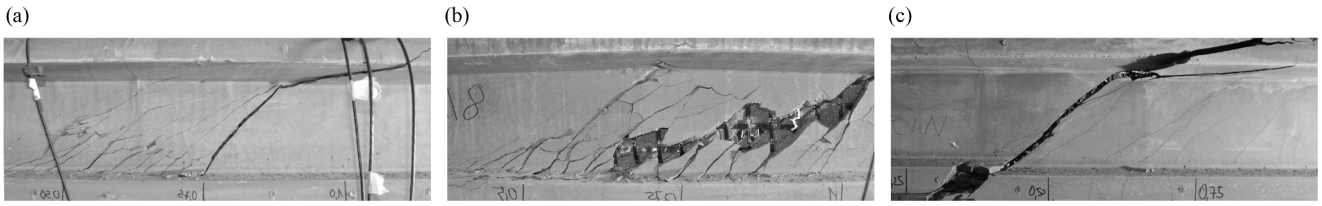

Fig. 5. Crack pattern at failure for TRC specimen: (a) reinforced with ASA-impregnated textile; (b) reinforced with epoxy impregnated textile; (c) reinforced with ASA-impregnated textile and prestressed CFRP rods [30].

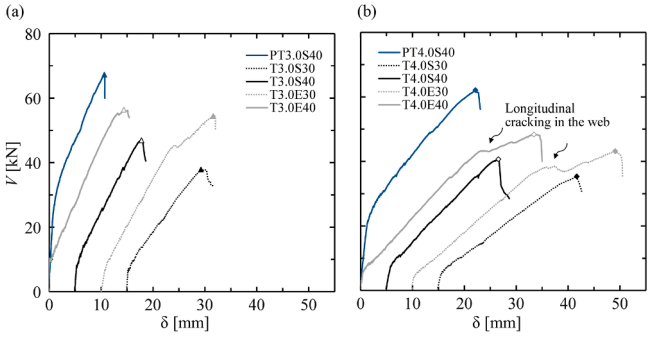

Fig. 6. Shear force–deflection diagram: (a) a/d ratio of about 3.0 (b) a/d ratio of about 4.0.

crack (e.g. a shear crack or a flexural crack) for textiles type 2 used in the experimental investigations (mean value of 0.20 mm for specimens with a web thickness of 30 mm and 0.24 mm for specimens with a web thickness of 40 mm), while for the ASA-impregnated textiles (type 1) the crack opening at failure is significantly bigger (mean value of 0.56 mm for both web thicknesses).

The crack opening results from the slip on both sides and the elastic elongation in between the crack opening (see Eq. (1)).

$$w = 2 \cdot \delta_b \cdot \left(1 + \frac{\sigma_{sw}}{E_{sw}}\right) \tag{1}$$

For the calculation of the stress state with a given (measured) crack opening, the bond slip at the crack is needed. This value is obtained by numerically integrating the differential equation of the relocatable slip (see Eq. (2), with τ(s) being the bond-slip relationship derived from the bond performance tests described in section 2.3.2 (see also Fig. 4, respectively Fig. 10).

$$\frac{ds^2(x)}{dx^2} - \frac{U_{tex}}{E_{tex} \cdot A_{rov}} \cdot \tau(s(x)) = 0 \tag{2}$$

The obtained stress-crack opening diagrams for both types of textile reinforcements are depicted in Fig. 8c.

4.2. Evaluation of shear strength due to textile reinforcement

By means of the stress-crack-opening diagrams given in section 4.1, the stress state in the fabric at failure $\sigma_{tex,eff}$ was evaluated for all test specimens. The calculated data is given in Table 5. It can be seen that the stress state at failure is significantly lower for the epoxy impregnated textiles when looking at it in relation to its higher tensile strength. In addition, the inclination of the critical shear crack was also evaluated and is listed for all specimens in Table 5. The method of determination of the critical shear crack inclination β_{cr} is depicted in Fig. 9 (a). The typical curved form of the shear crack was idealized with a straight line which connected the junction of the crack with top and lower flange. The shear carrying capacity of the textile reinforcement was then calculated according to Eq (3).

$$V_{R,tex} = \rho_w \cdot b_w \cdot (d - c) \cdot \sigma_{tex,eff} \cdot \cot\beta_{cr} \tag{3}$$

The calculated values of the shear resistance $V_{R,tex}$ are given in Table 5. In Fig. 9 (b) and (c) the shear carrying capacity of the textile reinforcement is graphically illustrated as part of the shear resistance of the specimens – V_{exp} in the case of the ASA-impregnated textiles and V_{spal} in the case of the epoxy-impregnated textiles. It can be seen, that the shear resistance of the textile reinforcement $V_{R,tex}$ was accountable for almost the full shear resistance, while the shear carrying capacity of the concrete $V_{R,c}$ was comparably low. The contribution of the textile reinforcement varied between 54% and 98% of the shear strength of the beams. Furthermore, the relation of the attribution of the fabrics to the shear carrying capacity decreased with an increasing width of the web and the depth of the top flange. A possible physical explanation could be the effect of the compression flange (acting as Timoshenko-beam) as the

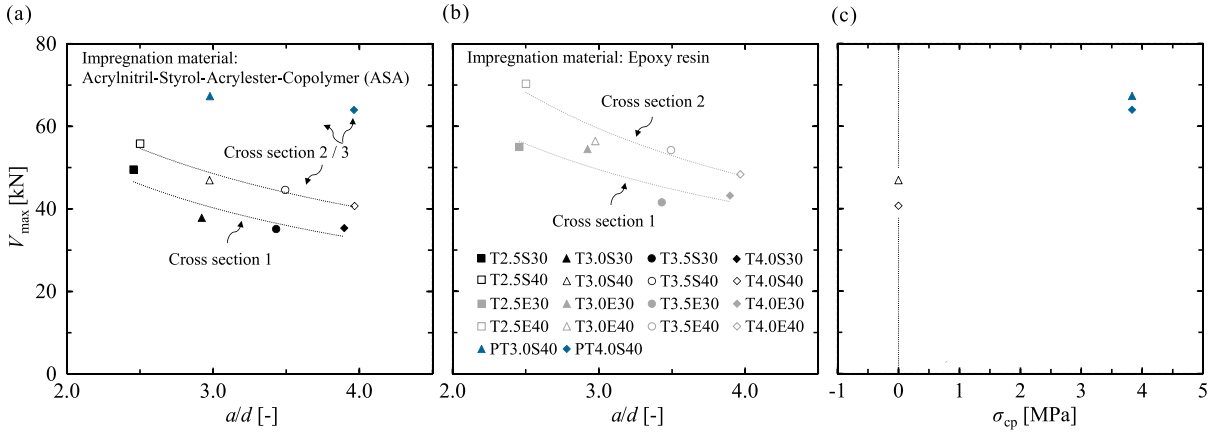

Fig. 7. Maximum shear force in the tests (V_{exp}) versus various influencing parameters: (a) a/d ratio for ASA impregnation (b) a/d ratio for epoxy resin impregnation (c) normal stresses due to prestressing $\sigma_{cp} = P_{test}/A_c$ [30].

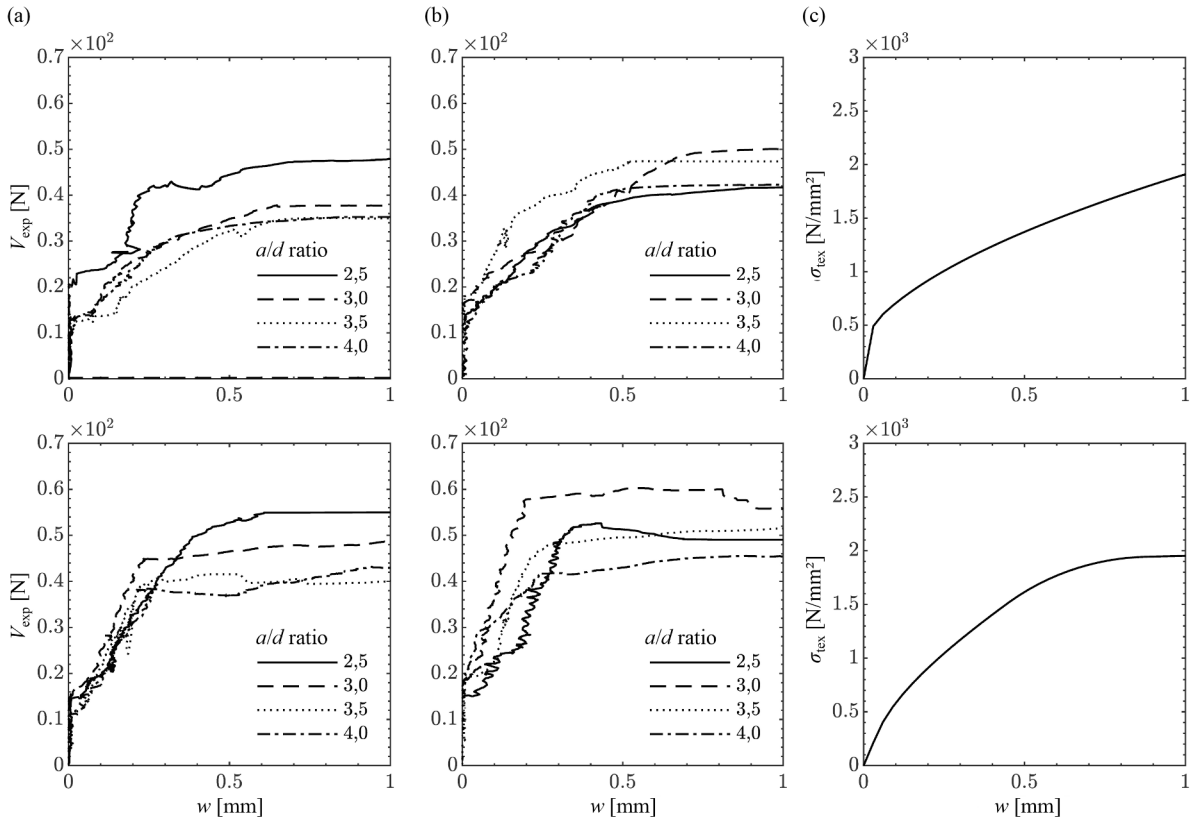

Fig. 8. Development of crack opening (representative measurement at one fibre strand) in relation to acting shear force for specimens with a web thickness of (a) 30 mm and (b) 40 mm as well as (c) the calculated stress-crack-opening diagram for ASA-impregnated textiles (type 1; top) and epoxy impregnated textiles (type 2; bottom).

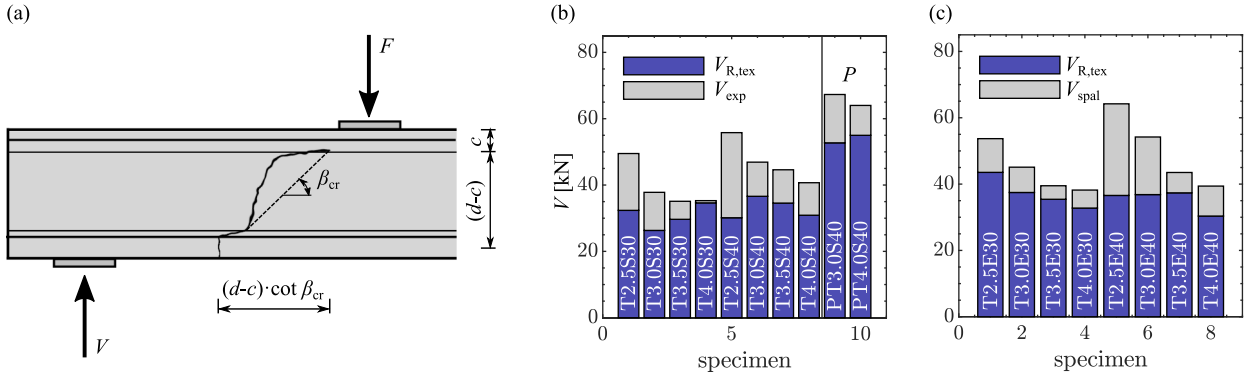

Fig. 9. (a) Determination of angle of critical shear crack, (b) shear carrying capacity of ASA-impregnated textiles as part of experimentally determined total shear carrying capacity, (c) shear carrying capacity of epoxy-impregnated textiles as part of determined shear resistance till spalling of the concrete cover occurs.

shear-transfer action takes over. Generally, it must be stated, that the shear-transfer actions for beams with moderate shear slenderness (a/d ratio > 3.0 for tests with point loads) contributed to concrete (e.g. [45]) are rather negligible. Moreover, the small aggregate size in combination with the relatively large crack openings, normally results in little contributions of aggregate interlock as well as shear strength in the fracture process zone. In addition, the dowelling effects of the longitudinal CFRP rods are not pronounced [9], with no dowelling cracks observed along the rebars during testing. On the other hand the shear strength due to arching action plays a very important role in beams with a low shear slenderness. A possible way to take this effect into account, is to use strut-and-tie models [46] or to increase the shear resistance by the factor $\beta = 3/(a/d)$ if a/d is smaller than 3 [47].

4.3. Efficiency of used textile reinforcement

In Fig. 10b the bond stress τ_b acting at the interface between the textile and the surrounding cementitious matrix is depicted for a shear crack crossing the fabric with an angle of α_{cr}. Additionally the force progression in the textile F_{tex} (Fig. 10c) as well as the concrete F_c (Fig. 10d) can be seen. The used textiles in the experimental programme exhibit significantly different bond behaviours. While the ASA-impregnated textiles (type 1) are able to transfer bond stresses due to friction once the maximum bond stress τ_b is reached, the bond performance of the epoxy impregnated textiles (type 2) is achieved by mechanical interlock. Due to the mechanical interlock, high splitting tensile stresses occur, which lead to a concrete failure once $F_{c,spal}$ is surpassed.

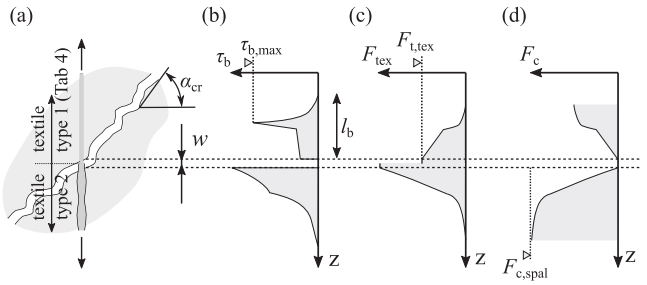

Fig. 10. Bond behaviour of textile reinforcement if a shear crack propagates and force progression in the concrete as well as in the textile fabric: ASA-impregnated textiles (top half) and epoxy-impregnated textiles (bottom half); (b) bond stress at anchorage, (c) force development in textile fabric, (d) force development in concrete.

Splitting tensile stresses are significantly less distinct for the ASA-impregnated textiles resulting in failure once the textile tensile strength $F_{t,tex}$ is reached. The reduction in the tensile strength in comparison to the uniaxial tensile tests can be mainly traced back to the inclined direction of the crack and the resulting non-uniaxial loading of the textile. This phenomenon leads, in the case of the prestressed specimens, to a higher efficiency factor due to the less steep inclination of the critical shear crack compared to that of non-prestressed specimens.

With the method described in section 4.1 a stress state in the textile reinforcement at failure for the epoxy impregnated textiles of approx. 900 MPa for a web thickness of 30 mm (crack width at failure of 0.20 mm; specimen T2.5E30 excluded as no excessive spalling was observed in this case) and 1000 MPa for a web thickness of 40 mm (crack width at failure of 0.24 mm) was calculated. This corresponds to an efficiency factor when related to the tensile strength of the fabrics of 0.27 and 0.30 respectively. The results are also in accordance with the bond performance tests described in section 2.3.2, as they exhibited an equivalent stress state in the fabric at failure. The same method is chosen for the ASA-impregnated textiles. The stress state at failure of approx. 1700 MPa is calculated. This corresponds to an efficiency factor of 0.82 for both web thicknesses of the non-prestressed specimens as well as the prestressed specimens (crack width at failure of 0.56 mm). As it can be seen here, the effectiveness of ASA impregnated textiles in this case is much higher than of the epoxy impregnated fabrics with a high yarn count. This correlates with the shear carrying capacity, as the enhancement of the shear carrying capacity between ASA impregnated textiles to those impregnated with epoxy resin was on average only 23% although the shear performance factor was more than four times higher.

The lower effectiveness of both textile fabrics will be considered in the following by specifying the textile stress $\sigma_{tex,eff}$ that can be transmitted via the shear crack. As the lower level of effectiveness in the case of the two impregnation materials are resting upon two different mechanisms, the effectiveness is considered with two different reduction factors, see Eq. (4).

$$\sigma_{tex,eff} = \min\{k_b, k_T\} \cdot f_{t,tex} \tag{4}$$

In the case of epoxy impregnated textiles a bond reduction factor k_b is introduced, which considers a premature shear failure of the specimen induced by a longitudinal cracking in the web in the layer of the textile fabric. For ASA-impregnated textiles the reduced effectiveness of the reinforcement is considered by a reduction factor k_T implemented on the textile strength, which is primary influenced by the non-uniaxial loading of the fabrics as in the past it was shown that the tensile strength of the fabrics decreases with increasing deviation from a uniaxial load condition. Nonetheless also other effects that may decrease the tensile strength of the fabric can be considered within factor k_T as for example an unfavourable folding radius of the fabric. In Table 6 the suggested parameters k_b and k_T on the base of measured crack openings in this study are summarized.

Table 6
Suggested parameters k_b and k_T for textile reinforcement used in this study.

	b_w	k_b	k_T
ASA	30	1.00	0.80
	40	1.00	0.80
Epoxy	30	0.25	–
	40	0.30	–

As the initiation of a spalling is dependent upon the resistance of the concrete, bond reduction factor k_b is influenced by the web thickness and has to be currently determined experimentally for every different combination of concrete and textile characteristics, e.g. by the bond performance test described in section 2.3.2. Amongst other parameters influencing the initiation of spalling (e.g. the compression force in the concrete cover, tension force in the out-of-plane direction), it was shown that the geometry of the fibre strand is a decisive parameter influencing the size and magnitude of the resulting splitting forces due to bond action [40], which lead the aforementioned longitudinal cracking. Alternatively the efficiency factor can be calculated by means of numerical solution of the differential equation of the relocatable slip and comparison of the resulting splitting tensile stresses with a concrete resistance against spalling, as it was described in [48]. As no spalling of the concrete cover was observed in the case of ASA-impregnated textiles, factor k_b was therefore set to be one in size. In contrast, factor k_T is only dependent upon the textile characteristics, therefore it can be determined for different fabrics individually and subsequently used for the calculation of other building components. As for epoxy impregnated textiles no rupture of the fabrics was observed in this study, parameter k_T was only determined for the ASA-impregnated textiles in this case.

5. Conclusions

In the course of a research project at TU Wien, ultra-high performance concrete (UHPC) and carbon reinforcement (textiles and rods) were combined to create lightweight, sustainable thin-walled structural elements. In this paper a test series investigating the shear performance of such elements, specifically T-beams with and without prestressed CFRP rods, is presented. Based on the influencing parameters investigated and the results obtained, the following conclusions can be drawn:

- The shear carrying capacity differs widely depending on the used textile reinforcement and the web and flange thickness of the T-beams. A thicker web and flange brings an improvement in the shear carrying capacity of around 20%. The shear carrying capacity of the epoxy-impregnated textiles was noted to be higher by only 23% in average compared to that of the ASA-impregnated textiles with the shear performance factor surpassing it by the factor four. It is noticeable that prestressing of the CFRP rods is an efficient way to improve the structural behaviour of thin-walled carbon textile reinforced T-beams. This is especially evident in the shear carrying capacity.
- Based on the DIC-measurements the crack width of the critical shear crack was evaluated and the stress state within the textile fabrics was calculated under consideration of bond models derived from bond performance tests. It was seen, that in both cases the uniaxial tensile strength of the fabrics could not be fully exploited. While there is a reduction of the tensile strength of the fabrics due to a non-axial loading for the ASA-impregnated textiles, the specimens reinforced with epoxy-resin impregnated textile shear reinforcement tend to fail at an early load stage due to a spalling of the concrete cover in the web. As a consequence, the high tensile strength of the reinforcement cannot be exploited efficiently. As shown in various studies this failure mechanism can be tracked down to high splitting tensile stresses [40].

- In contrast to steel-reinforced concrete, where longitudinal cracking is avoided by minimum values of concrete cover or a minimum amount of shear reinforcement overlapping the longitudinal reinforcement, such detailing would often oppose the design philosophy of TRC of thin-walled filigree structural components. The focus therefore should lie on the consideration of the reduced effectiveness of the textile reinforcement by means of appropriate design models. However, if the utilization rate is too low, it is possible that, in view of the high price of the material, economic efficiency may no longer be guaranteed. This design philosophy will therefore lead to a balancing act between reduced efficiency of the textile reinforcement on the one hand, and a reduction of concrete consumption on the other.
- The determination whether a TRC-component tends to concrete spalling can either be done experimentally using a SPO-test with adaptions according to Bielak et al. [39], or by design models (see for example [49]). The lower effectiveness of textile fabrics can then be considered by specifying the textile stress $\sigma_{tex,eff}$ that can be transmitted via the shear crack. As the lower level of effectiveness in the case of ASA-impregnated textiles and epoxy-impregnated textiles rest upon different mechanisms, the two efficiency factors k_b and k_T are introduced. While factor k_b considers a premature shear failure of the specimen induced by a longitudinal cracking in the web, factor k_T accounts for different mechanisms which reduce the breaking strength of the textile reinforcement (for example an unfavourable folding radius of the fabric).

CRediT authorship contribution statement

Philipp Preinstorfer: Conceptualization, Methodology, Validation, Formal analysis, Investigation, Data curation, Writing - original draft, Writing - review & editing, Visualization. **Patrick Huber:** Conceptualization, Methodology, Validation, Formal analysis, Investigation, Writing - original draft, Visualization, Supervision. **Tobias Huber:** Validation, Formal analysis. **Benjamin Kromoser:** Conceptualization, Validation, Investigation, Supervision, Project administration, Funding acquisition. **Johann Kollegger:** Validation, Supervision.

Declaration of Competing Interest

The authors declared that there is no conflict of interest.

Acknowledgements

The authors want to express their sincere gratitude to the Austrian Research Promotion Agency (FFG) for the financial support [Grant Nr.: 851270]. They also want to thank the companies Solidian GmbH for providing the textile reinforcement, the company SW Umwelttechnik AG for the production of the test specimens and the Institute for Lightweight Structures and Conceptual Design (ILEK) at the University of Stuttgart for the good cooperation. The authors acknowledge TU Wien Bibliothek for financial support through its Open Access Funding Programme.

Data availability

The data supporting the findings of this study are available on request from the corresponding author.

References

[1] Hegger, J., Sonderforschungsbereich 532 - Textilbewehrter Beton - Grundlagen für die Entwicklung einer neuartigen Technologie: Abschlussbericht., RWTH Aachen, 2012.
[2] Curbach M, Ortlepp R. Sonderforschungsbereich 528 - Textile Bewehrungen zur bautechnischen Verstärkung und Instandsetzung: Abschlussbericht. TU Dresden 2011.
[3] Portal NW, Lundgren K, Wallbaum H, Malaga K. Sustainable Potential of Textile-Reinforced Concrete. J Mater Civ Eng 2015;27:04014207. https://doi.org/10.1061/(ASCE)MT.1943-5533.0001160.
[4] Si Larbi A, Agbossou A, Hamelin P. Experimental and numerical investigations about textile-reinforced concrete and hybrid solutions for repairing and/or strengthening reinforced concrete beams. Compos Struct 2013;99:152–62. https://doi.org/10.1016/j.compstruct.2012.12.005.
[5] Yin S, Xu S, Lv H. Flexural Behavior of Reinforced Concrete Beams with TRC Tension Zone Cover. J Mater Civ Eng 2014;26:320–30. https://doi.org/10.1061/(ASCE)MT.1943-5533.0000811.
[6] Hegger J, Voss S. Investigations on the bearing behaviour and application potential of textile reinforced concrete. Eng Struct 2008;30:2050–6.
[7] Curbach M, Jesse F. Specifications and Application of Textile Reinforced Concrete (TRC). Beton- Stahlbetonbau 2009;104:9–16. https://doi.org/10.1002/best.200800653.
[8] Kirsten M, Freudenberg C, Cherif C. Carbon Fibers, material of the 21st century. Beton- Stahlbetonbau 2015;110:8–15. https://doi.org/10.1002/best.201400105.
[9] El Ghadioui R, Proske T, Tran NL, Graubner C-A. Structural behaviour of CFRP reinforced concrete members under bending and shear loads. Mater Struct 2020;53:63. https://doi.org/10.1617/s11527-020-01496-7.
[10] Preinstorfer P, Kromoser B, Kollegger J. Flexural behaviour of filigree slab elements made of carbon reinforced UHPC. Constr Build Mater 2019;199:416–23. https://doi.org/10.1016/j.conbuildmat.2018.12.027.
[11] Egger M, Feix J. Gestickte textile Bewehrungen für die Beton-Leichtbauweise, Beiträge zur 5. DAfStb-Jahrestagung mit 58. Forschungskolloquium - Forschungskolloquium Band1. TU Kaiserslautern 2017:110–21.
[12] Bielak J, Schmidt M, Hegger J, Jesse F. Structural Behavior of Large-Scale I-Beams with Combined Textile and CFRP Reinforcement. Applied Sciences 2020;10. https://doi.org/10.3390/app10134625.
[13] Hamilton III H, Dolan C. Durability of FRP reinforcements for concrete. Prog Struct Mat Eng 2000;2:139–45. https://doi.org/10.1002/1528-2716(200004/06)2:2<139::Aid-pse17>3.0.Co;2-3.
[14] Hegger J, Goralski C, Kulas C. A pedestrian bridge made of textile reinforced concrete. Beton- Stahlbetonbau 2011;106:64–71. https://doi.org/10.1002/best.201000081.
[15] Scholzen A, Chudoba R, Hegger J. Thin-walled shell structures made of textile-reinforced concrete. Structural Concrete 2015;16:106–14. https://doi.org/10.1002/suco.201300071.
[16] Sharei E, Scholzen A, Hegger J, Chudoba R. Structural behavior of a lightweight, textile-reinforced concrete barrel vault shell. Compos Struct 2017;171:505–14. https://doi.org/10.1016/j.compstruct.2017.03.069.
[17] Berger, J.; Gericke, O.; Feix, J.; Sobek, W.: Experimental investigations on actively bent concrete shells. Structural Concrete Early-View. doi: 10.1002/suco.202000045.
[18] Hegger J, Kulas C, Horstmann M. Spatial Textile Reinforcement Structures for Ventilated and Sandwich Facade Elements. Adv Struct Eng 2012;15:665–75. https://doi.org/10.1260/1369-4332.15.4.665.
[19] Kromoser B, Gericke O, Sobek W. Implants for load introduction into thin-walled CFRP-reinforced UHPC beams. Compos Struct 2018;194:178–87. https://doi.org/10.1016/j.compstruct.2018.03.044.
[20] Kromoser B, Preinstorfer P, Kollegger J. Building lightweight structures with carbon-fiber-reinforced polymer-reinforced ultra-high-performance concrete: Research approach, construction materials, and conceptual design of three building components. Structural Concrete 2019;20:730–44. https://doi.org/10.1002/suco.201700225.
[21] Curbach M, Hauptenbuchner B, Ortlepp R, Weiland S. Textile reinforced concrete for strengthening of a hypar shell structure in Schweinfurt. Beton- Stahlbetonbau 2007;102:353–61. https://doi.org/10.1002/best.200700551.
[22] Ortlepp R, Ortlepp S. Textile reinforced concrete for strengthening of RC columns: A contribution to resource conservation through the preservation of structures. Constr Build Mater 2017;132:150–60. https://doi.org/10.1016/j.conbuildmat.2016.11.133.
[23] Brückner A, Ortlepp R, Curbach M. Anchoring of shear strengthening for T-beams made of textile reinforced concrete (TRC). Mater Struct 2008;41:407–18. https://doi.org/10.1617/s11527-007-9254-9.
[24] Herbrand M, Claßen M, Hegger J. Querkraftversuche an Spannbetonträgern mit carbontextilbewehrter Spritzmörtelverstärkung unter zyklischer Beanspruchung. Beton- Stahlbetonbau 2016;111:576–87. https://doi.org/10.1002/best.201600010.
[25] Younes A, Seidel A, Rittner S, Cherif C, Thyroff R. Innovative textile reinforcements for concrete applications. Beton-und Stahlbetonbau 2015;110:16–21. https://doi.org/10.1002/best.201400101.
[26] Valeri P, Fernàndez Ruiz M, Muttoni A. Tensile response of textile reinforced concrete. Constr Build Mater 2020;258:119517. https://doi.org/10.1016/j.conbuildmat.2020.119517.
[27] Kulas, C.: Zum Tragverhalten getränkter textiler Bewehrungselemente für Betonbauteile. RWTH Aachen, doctoral thesis. 2014.
[28] Stoiber N, Hammerl M, Kromoser B. Cradle-to-gate life cycle assessment of CFRP reinforcement for concrete structures: calculation basis and exemplary application. J Cleaner Prod 2020. https://doi.org/10.1016/j.jclepro.2020.124300.
[29] Rempel, S.; Ricker, M.; Hegger, J.: Design model with an iterative and closed approach for textile reinforced concrete structures with bending load – clear bending load and a combination with normal force. Beton- und Stahlbetonbau n/a. doi: 10.1002/best.201900086.

[30] Kromoser, B.; Huber, P.; Preinstorfer, P., Experimental study of the shear load bearing behaviour of thin walled CFRP reinforced UHPC structures, fib congress 2018 - better, smarter, stronger, Melbourne, 2018, pp. 364-365.
[31] Markunovic N. Untersuchungen zum Vorspannen filigraner UHPC-Bauteile mit CFK-Stäben. Master thesis. Wien 2017.
[32] AFGC. Ultra High Performance Fibre-Reinforced Concretes, Recommendations. AFGC/ SETRA 2013.
[33] ÖNORM EN 196-1, Methods of testing cement – Part 1: Determination of strength, Austrian Standards Institute (ON), Vienna, 2005.
[34] Schütze E, Bielak J, Scheerer S, Hegger J, Curbach M. Uniaxial tensile test for carbon reinforced concrete with textile reinforcement. Beton- Stahlbetonbau 2018; 113:33–47. https://doi.org/10.1002/best.201700074.
[35] Preinstorfer P, Kromoser B, Kollegger J. Influencing parameters on longitudinal cracking in textile reinforced concrete. Beton- Stahlbetonbau 2018;113:877–85. https://doi.org/10.1002/best.201800071.
[36] Preinstorfer P, Kromoser B, Kollegger J. Categorisation of the bond behaviour of textile reinforced concrete. Bauingenieur 2019;94:416–24.
[37] TC RILEM.: RILEM recommendations for the testing and use of constructions materials. RC 6 bond test for reinforcement steel. 2. Pull-out test (1983), pp. 218-220.
[38] Lorenz E, Schütze E, Schladitz F, Curbach M. Textile Reinforced Concrete – Overview of standard test methods. Beton- Stahlbetonbau 2013;108:711–22. https://doi.org/10.1002/best.201300041.
[39] Bielak J, Spelter A, Will N, Claßen M. Anchorage behavior of textile reinforcement in thin concrete components. Beton- Stahlbetonbau 2018;113:515–24. https://doi.org/10.1002/best.201800013.
[40] Preinstorfer P, Kollegger J. New insights into the splitting failure of textile-reinforced concrete. Compos Struct 2020;243:1–10. https://doi.org/10.1016/j.compstruct.2020.112203.
[41] Preinstorfer P. Zur Spaltrissbildung von textilbewehrtem Beton. TU Wien academic press 2020. https://doi.org/10.34727/2020/isbn.978-3-85448-034-1.
[42] Richter M. Entwicklung mechanischer Modelle zur analytischen Beschreibung der Materialeigenschaften von textilbewehrtem Feinbeton. TU Dresden, Dissertation. 2005.
[43] Li Y, Bielak J, Hegger J, Chudoba R. An incremental inverse analysis procedure for identification of bond-slip laws in composites applied to textile reinforced concrete. Compos B Eng 2018;137:111–22. https://doi.org/10.1016/j.compositesb.2017.11.014.
[44] Preinstorfer P, Kromoser B, Kollegger J. Development of prestressed T-beams made of textile reinforced UHPC. 39th IABSE Symposium - Engineering the future 2017: 3130–5.
[45] Huber P, Huber T, Kollegger J. Investigation of the shear behavior of RC beams on the basis of measured crack kinematics. Eng Struct 2016;113:41–58. https://doi.org/10.1016/j.engstruct.2016.01.025.
[46] Schlaich J. Zum einheitlichen Bemessen von Stahlbetontragwerken. Beton-Stahlbetonbau 1984;79:89–96. https://doi.org/10.1002/best.198400160.
[47] Huber P, Huber T, Kollegger J. Experimental and theoretical study on the shear behavior of single- and multi-span T- and I-shaped post-tensioned beams. Structural Concrete 2020;21:393–408. https://doi.org/10.1002/suco.201900085.
[48] Preinstorfer P, Pinzek A, Kollegger J. Modellierung des Verankerungsverhaltens getränkter textiler Bewehrungen. Beton- Stahlbetonbau 2020;115. https://doi.org/10.1002/best.202000011.
[49] Preinstorfer P, Kromoser B. Influence of geometrical parameters on the splitting forces in textile-reinforced concrete. Materials and Structures 2020;53(6):1–17. https://doi.org/10.1617/s11527-020-01590-w.